

## Externally Driven Nonlinear Time-Variant Metasurfaces

Varvara V. Zubyyuk,\* Pavel A. Shafirin, Maxim R. Shcherbakov, Gennady Shvets, and Andrey A. Fedyanin

Cite This: *ACS Photonics* 2022, 9, 493–502

Read Online

ACCESS |



Metrics &amp; More



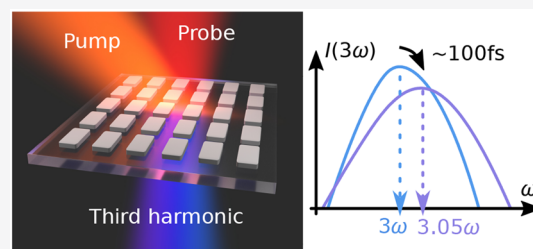
Article Recommendations



Supporting Information

**ABSTRACT:** Resonant photonic nanostructures exhibiting enhanced nonlinear response and efficient frequency conversion are an emergent platform in nonlinear optics. High-index semiconductor metasurfaces with rapidly tuned high-quality-factor (high-Q) resonances enable a novel class of time-variant metasurfaces, which expands the toolbox of color management at the nanoscale. Here, we report on the dynamic control of the nonlinear optical response in time-variant semiconductor metasurfaces supporting high-Q resonances in the near-infrared spectral range. Germanium metasurfaces reveal frequency conversion of the fundamental beam and blue-shift of 10 nm ( $3.05\omega$ ) and 40% broadening in the third-harmonic spectrum due to a subpicosecond-scale time-variant refractive index. A time-dependent coupled-mode theory, in qualitative agreement with the experimental data, validated the time-variant nature of the system. Our findings expand the scope of time-variant metasurfaces and may serve as base for the next generation of nanoscale pulse shapers, optical switches, and light sources.

**KEYWORDS:** metasurfaces, nonlinear optics, time-variant materials, ultrafast processes, high-Q resonances, all-optical modulation



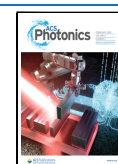
Metasurfaces, arrays of periodically arranged nanoparticles,<sup>1,2</sup> have established themselves as a promising alternative for various optics elements like lenses,<sup>3</sup> holograms,<sup>4,5</sup> deflectors,<sup>6,7</sup> and polarizers.<sup>2</sup> As an emergent platform in nonlinear optics, resonant photonic nanostructures revealed an enhanced nonlinear response and efficient frequency conversion.<sup>6,8–15</sup> One of the downsides of metasurfaces is their fixed optical properties, imposing restrictions on their use after fabrication. Many works were dedicated to active and tunable metasurfaces, where an external stimulus changes the properties of the structures. As such, mechanical,<sup>16</sup> electrical,<sup>17,18</sup> or thermal control,<sup>19</sup> optical excitation,<sup>20–22</sup> magneto-optical control,<sup>23–25</sup> use of phase-change materials,<sup>26,27</sup> or chemical approaches<sup>28</sup> and hybrid systems like liquid crystals<sup>29,30</sup> can tune the spectral position of metasurfaces' resonances. Many of the potential applications of metasurfaces, especially in nonlinear and tunable cases, require sharp spectral features and high local electric fields. To fulfill these conditions, Mie-type resonances are widely used,<sup>31</sup> first demonstrated in high-index particles with spherical form and other shapes such as disc-shaped particles.<sup>1,32</sup> Individual resonant nanoparticles can be combined into strongly coupled arrays, where high-quality-factor (high-Q) modes enable metasurfaces with sharp spectral features and enhanced light–matter interactions,<sup>33,34</sup> leading to many exciting applications.<sup>35,36</sup> Using high-Q structures, photonic devices with properties beyond what is available with bulk materials and low-Q metasurfaces can be attained.<sup>37–39</sup> High-index semiconductor metasurfaces with specially designed high-Q resonances have great capability for enhanced nonlinear optical

effects and other benefits for creating various compact nonlinear photonics devices.

In the extreme case where resonances of metasurfaces are tuned rapidly, a novel class of effects pertaining to the time-variant nature of metasurfaces emerges. Under this framework, harmonic waves cease to be solutions of Maxwell's equations, and effects such as frequency conversion,<sup>40–42</sup> photon acceleration,<sup>39</sup> nonreciprocal light reflection, beam steering, or focusing<sup>43–45</sup> that are impossible in stationary systems rise, similar to original works in rapidly generated plasmas.<sup>46,47</sup> The frequency conversion that has recently been shown for metasurfaces also has origins similar to that of the coherent artifact in ultrafast time-resolved infrared (IR) spectroscopy of vibrational transitions in chemical systems<sup>48,49</sup> and for semiconductors,<sup>50,51</sup> which manifest at negative pump–probe time delays when the probe pulse precedes the pump pulse. Even though many systems have revealed linear frequency conversion due to abrupt time modulation, ultrafast studies of the nonlinear response,<sup>52–55</sup> which are prominent in resonant metasurfaces, are yet to unveil the control of light frequency for nonlinearly generated waves. This concept bears significant importance for attosecond physics and high harmonic generation, where isolated attosecond pulses benefit from spectrally alternated harmonic signals.<sup>56</sup>

Received: August 11, 2021

Published: January 20, 2022



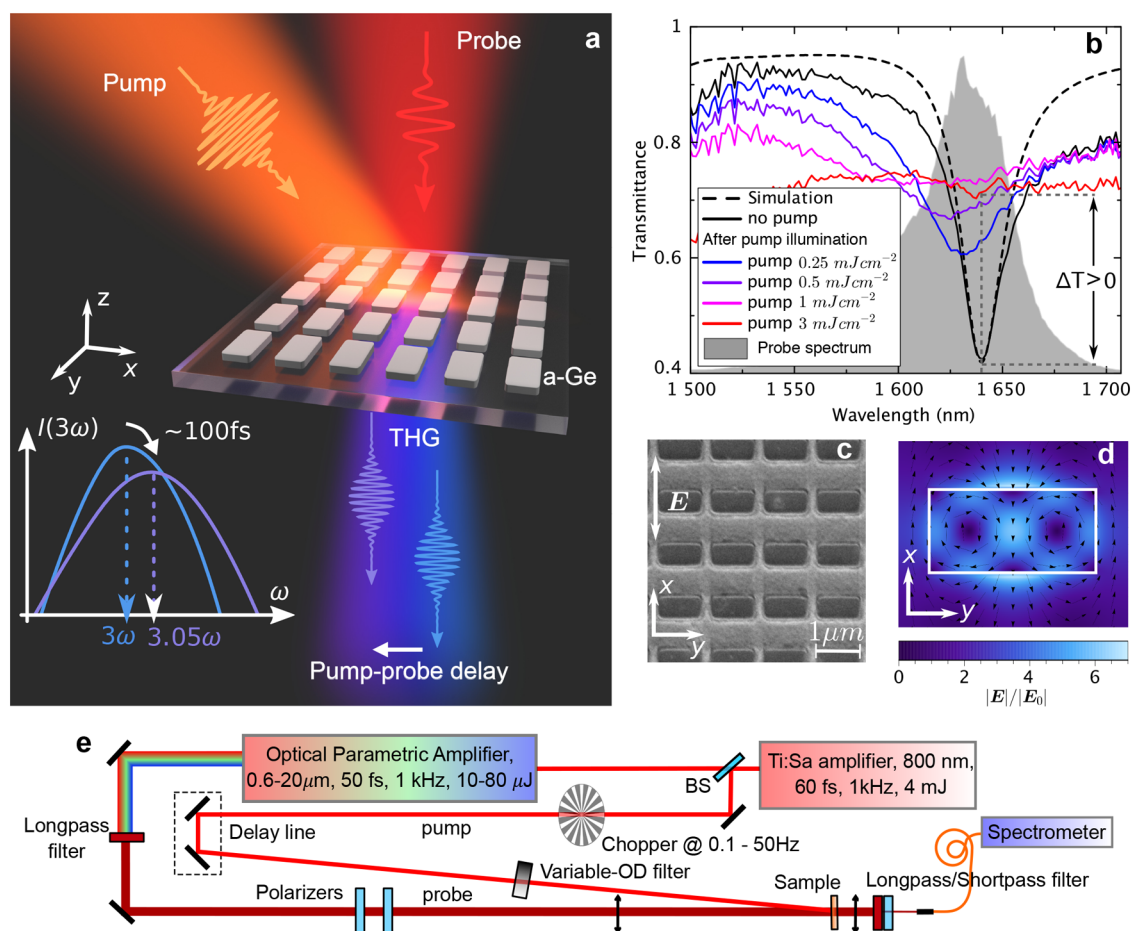


**Figure 1.** External optical drive enables time-variant resonances in a nonlinear germanium metasurface. (a) The concept of optically driven nonlinear response of a time-variant amorphous germanium (a-Ge) metasurface. The absorption of a pump pulse rapidly modifies the refractive index of a-Ge. As a result, the third-harmonic signal generated by the probe beam can get dynamically up-converted, following the fast evolution of the resonance. (b) The experimental and simulated transmittance spectra of the a-Ge metasurface in the absence of optical pumping (solid and dashed black curves, respectively) and transmittance spectra after illumination by various pump fluences at time delay  $\tau = 100$  fs (colored curves). The gray region shows the spectrum of the probe pulse. (c) A scanning electron microscope image of a typical metasurface sample (top view). The white arrow represents the polarization direction of the probe pulse. (d) A map of the simulated field amplitude  $|E|/|E_0|$  (color) and direction (black arrows) at the central wavelength of the metasurface resonance inside the a-Ge cuboid in horizontal cross-section of a cuboid exhibiting high local field enhancement pertaining to the high-Q resonance. (e) Schematic of pump–probe spectroscopy setup.

Here, we report on the dynamic control of the nonlinear optical response of a time-variant semiconductor metasurface. We design and experimentally implement a germanium-based metasurface that possesses a high-Q resonance in the near-infrared spectral range and exhibits a frequency conversion due to the rapidly photoinduced time-variant refractive index in a subpicosecond pump–probe experiment. Owing to the combination of the high-Q resonance and time-variant refractive index, the metasurface demonstrates blue-shifted and spectrally broadened fundamental beam and third-harmonic generation (THG) at negative pump–probe time delays. We observe a blue-shift of 10 nm and 40% broadening in the third-harmonic generation spectrum around a wavelength of 540 nm, as well as its complete suppression at positive delays. To model the experimental results, a coupled-mode theory is developed, which has confirmed the observed wavelength shifts and validated their time-variant nature. The observed external photoinduced control over the frequency of nonlinearly generated photons establishes a new utility for time-variant metasurfaces and opens opportunities for novel light sources at the nanoscale.

## RESULTS

**Metasurface Samples and Concept.** The work is conceptualized in Figure 1a. A semiconductor metasurface formed by an array of amorphous germanium (a-Ge) cuboids was chosen as a time-variant medium, and its capabilities as a frequency converter were investigated using pump–probe spectroscopy. Due to a-Ge cuboids located close to each other, the metasurfaces manifested high-Q resonances,<sup>35</sup> and a-Ge provided the free-carriers generation under the optical pump illumination and, therefore, enabled rapid changes of the refractive index; see Methods for the sample fabrication procedure. A scanning electron microscope (SEM) image of a typical metasurface (top view) is represented in Figure 1c: dark areas correspond to Ge. The Q-factor of the resonances depended on the size of the gap between the short sides of the cuboids and varied from 30 to 65. We chose the metasurface with  $Q = 65$  as a sample for this study. Its experimental and simulated transmittance spectra in the near-IR in the unperturbed regime are displayed in Figure 1b by solid and dashed black curves, respectively; see Methods for the

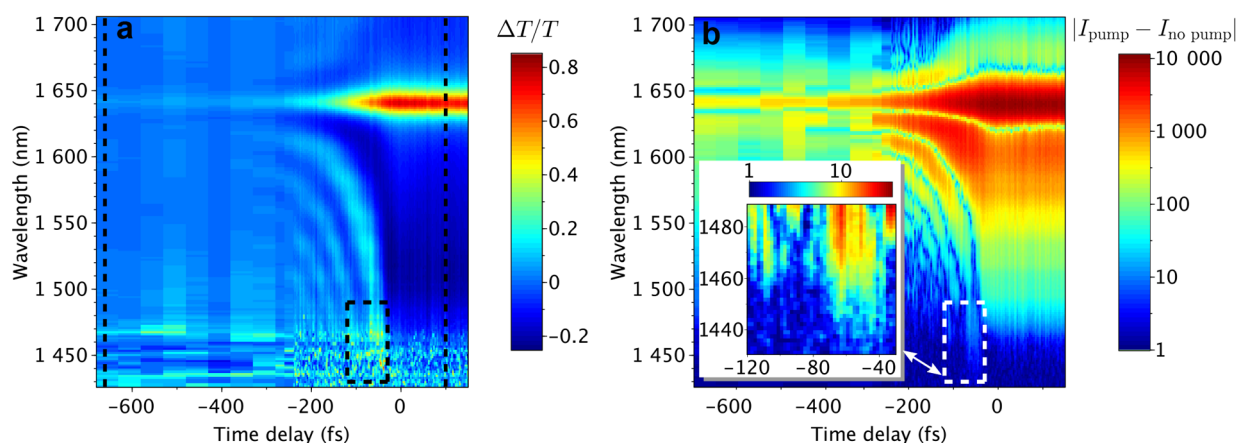


**Figure 2.** Experimental linear frequency conversion in a time-variant a-Ge metasurface. (a) Transient transmittance of a metasurface with the resonance at 1640 nm as a function of the probe wavelength and pump–probe delay. The dashed black rectangle denotes the zoom area for insert in (b); the vertical dashed lines correspond to  $\tau = -680$  fs (the resonance close to the unperturbed case:  $T_{-680} \approx T_{\text{no pump}}$ ) and  $\tau = 100$  fs (after pump illumination) for transmittance spectra in Figure 1b. (b) The difference between probe spectrum under pump illumination and without pump illumination, logarithmic scale, as a function of the probe wavelength and pump–probe delay. Inset: zoom of the dashed white rectangle area, showing new frequency components generated at wavelengths as short as 1450 nm.

calculation and measurement details. The polarization of the incident light was perpendicular to the long sides of the cuboids, depicted on the SEM image with a white arrow. The gray region denotes the spectrum of the incident probe pulse, which resonantly excited a magnetic quadrupolar Mie mode in the metasurface. A calculated field distribution inside the a-Ge cuboid at the resonant wavelength in Figure 1d demonstrates two electric field vortices that generate two out-of-phase, out-of-plane magnetic dipoles. The transmittance spectra after illumination by different pump fluence (colored curves) at pump–probe time delay  $\tau = 100$  fs exhibit a shift of the resonance and a decrease in its Q-factor due to the modification in the a-Ge refractive properties. These changes become more apparent with increasing the pump fluence, as more free-carriers are generated. For a pump fluence of  $1 \text{ mJ}/\text{cm}^2$  (pink curve), the resonance is still visible and experiences a blue-shift of about 30 nm. We estimate the resonance shift at a fluence of  $3 \text{ mJ}/\text{cm}^2$  to be approximately 100 nm.

**Transient Linear and Nonlinear Spectroscopy.** The ultrafast dynamics of infrared transmittance and third-harmonic generation signal were studied using the pump–probe technique. The setup is schematically shown in Figure 1e. Ti:sapphire amplified femtosecond pulses were used to pump the metasurface and induce rapid changes of the refractive index. The pulses from the optical parametric amplifier were used to probe the response of metasurfaces. The system ran at a low repetition rate of 1 kHz to minimize the residual pulse-to-pulse heating. The probe pulse duration was 50 fs and its central wavelength of 1640 nm was tuned to the metasurface resonance (gray area in Figure 1b). The pump pulse was 60 fs long, with a central wavelength of 800 nm and a fluence varied from 0.25 to  $3 \text{ mJ}/\text{cm}^2$ . The probe was focused under normal incidence, whereas the pump fell on the sample at a small off-normal angle; for experimental details, see Methods. The transmitted probe pulse spectra were measured both under and without the pump presence as a function of time delay  $\tau$  between the pump and probe pulses in the near-infrared and visible spectral ranges. The transient transmittance is defined as  $\Delta T/T = (T_{\text{pump}}(\tau) - T)/T = \Delta I/I = (I_{\text{pump}}(\tau) - I)/I$ , where  $T$  is the transmittance of the sample and  $I$  is the

laser spectrum of the probe passing through the sample in the absence of the pump pulse, and  $T_{\text{pump}}(\tau)$ ,  $I_{\text{pump}}(\tau)$  are the values under the pump illumination at the pump–probe time delay  $\tau$ .

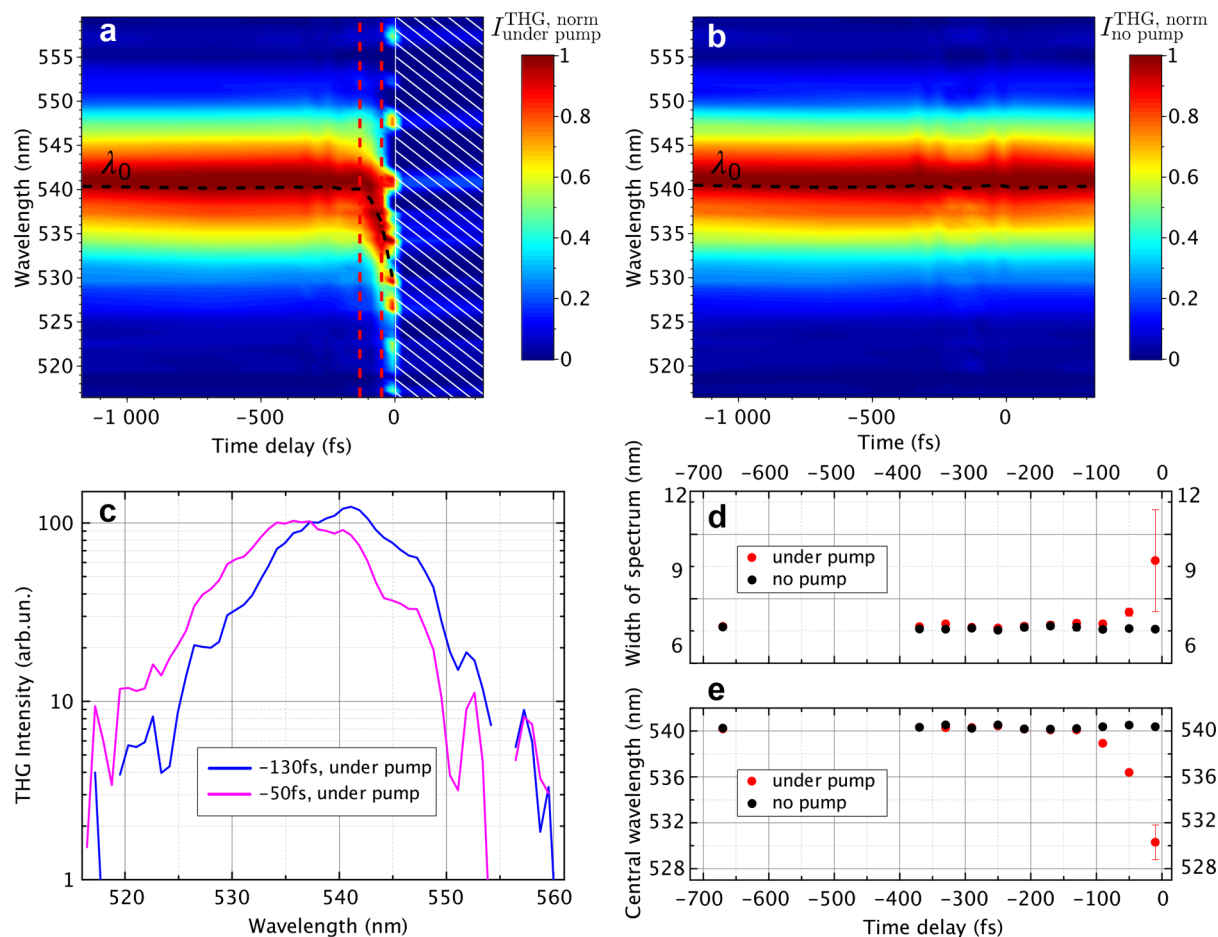
### Frequency Conversion in Fundamental Spectrum.

Figure 2a represents transient transmittance  $\Delta T/T$  for an a-Ge metasurface with the resonance at the central wavelength 1640 nm. A significant change in transmission is observed, with positive (up to +80% near the resonance central wavelength) and negative variation (down to −25%) in consequence of blue-shift and reduced Q-factor of the resonance in the transmittance spectrum (Figure 1b) due to the refractive index changes under the induced free carriers. In transient spectroscopy experiments, we focus on negative time delays close to zero delay, where the effects associated with the time-variant nature of the system can be observed.<sup>39–45</sup> The photoinduced modulation of the metasurface's resonance enables frequency conversion of the fundamental beam, as seen in Figure 2a,b, between −300 and 0 fs time delays. At such negative time delays, as a result of a long lifetime of the mode, characteristic fringes<sup>42,49,57</sup> can be observed. They originate from the interference between the resonant part of the probe that is being dynamically frequency-converted in the metasurface (the central part of the probe spectrum, which interacts with the resonance of the metasurface) and the nonresonant part of the probe (the edges of the probe spectrum that are outside of the metasurface resonance's bandwidth). The extent to which the new frequencies are generated in the metasurface through time variance can be appreciated at wavelengths far from both the unperturbed resonance and the probe carrier wavelength. The differential intensity plot in Figure 2b demonstrates that, at small negative pump–probe delays around −70 to −40 fs, the above-noise signal is generated at wavelengths as short as 1450 nm, that is about 200 nm away from the initial resonance position, signifying strong frequency conversion due to the time-variant nature of the metasurface.

### Frequency Conversion of the Third-Harmonic Signal.

The free-carrier-induced time-dependent refractive index of the metasurface imposes femtosecond dynamics in the THG response, causing conversion of the THG frequency. The





**Figure 3.** Frequency conversion of the harmonic response in a time-variant metasurface. The normalized spectra of the third-harmonic signal generated by the probe pulse under pump as a function of the pump–probe delay (a) and without pump illumination as a function of time (b). The black dashed lines indicate the position of central wavelength  $\lambda_0$  from (e). The vertical red dashed lines in (a) denote the time delays for the THG intensity spectra cross sections in (c). The hatched white rectangle marks the area with noisy signal that prevents meaningful normalization. (c) THG spectra under pump illumination at time delays  $\tau = -130$  fs (blue curve) and  $\tau = -50$  fs (pink curve). The extracted width of spectrum  $\sigma$  (d) and central wavelength  $\lambda_0$  (e) of the THG spectrum as functions of  $\tau$  under pump illumination (red dots) and without pump illumination (black dots).

experimental ultrafast all-optical nonlinear modulation of a-Ge metasurfaces is displayed in Figure 3a. The normalized third-harmonic signal generated by the probe pulse with a central wavelength of  $\lambda_{\text{probe}} = 1610$  nm under the pump illumination reveals a blue-shift of the THG wavelength at the femtosecond scale for negative pump–probe time delays. This blue-shift (or photon acceleration<sup>47</sup>) of the nonlinear signal occurs due to the negative term of the photodoped semiconductor refractive index that is proportional to the number of free carriers generated by the pump beam,  $\Delta n \propto -N_{\text{FC}}(t)$ . The hatched white rectangle marks the area with noisy signal that prevents meaningful normalization. The unperturbed a-Ge metasurface generates the third-harmonic signal with stable behavior in time but with small deviation in spectrum from delay to delay due to some instability of the probe laser (Figure 3b). These fluctuations are similar enough to each other for far from zero negative time delays and thus allows to conclude that such effect is not related to the time-variant nature of the system. Red dashed lines in Figure 3a denote the time delays for the THG intensity spectra cross sections in Figure 3c. Figure 3c represents unnormalized THG spectra at time delays  $\tau = -130$  and  $-50$  fs under pump illumination. The THG spectrum at  $\tau$

$= -130$  fs has similar parameters as all spectra for more negative delays and as unperturbed spectrum (without pump illumination). The THG signal exhibits blue-shift and broadening at negative delays near zero with values increasing with increasing the time delay. We fit the spectra in Figure 3a,b by a  $\text{sech}^2$  function:

$$y = y_0 + A \text{sech}^2\left(\frac{\lambda - \lambda_0}{\sigma}\right) \quad (1)$$

where  $y_0$  is the offset,  $A$  is the amplitude,  $\lambda_0$  is the central wavelength, and  $\sigma$  is the spectral full width at half-maximum. The extracted values of  $\sigma$  and  $\lambda_0$  as a function of  $\tau$  under pump illumination (red dots) and without pump illumination (black dots) are displayed in Figure 3d and e, respectively. The error bars of the data points that are not near zero delay are smaller than the data point markers. The blue-shift and broadening of the THG signal without the pump fluctuate due to the instabilities of the probe beam with characteristic deviation values less than the spectrum modification caused by the pump. The highest values of measured blue-shift and broadening of the THG spectrum are 10 nm and 40%, respectively, at  $\tau = -10$  fs. The blue-shift of 10 nm

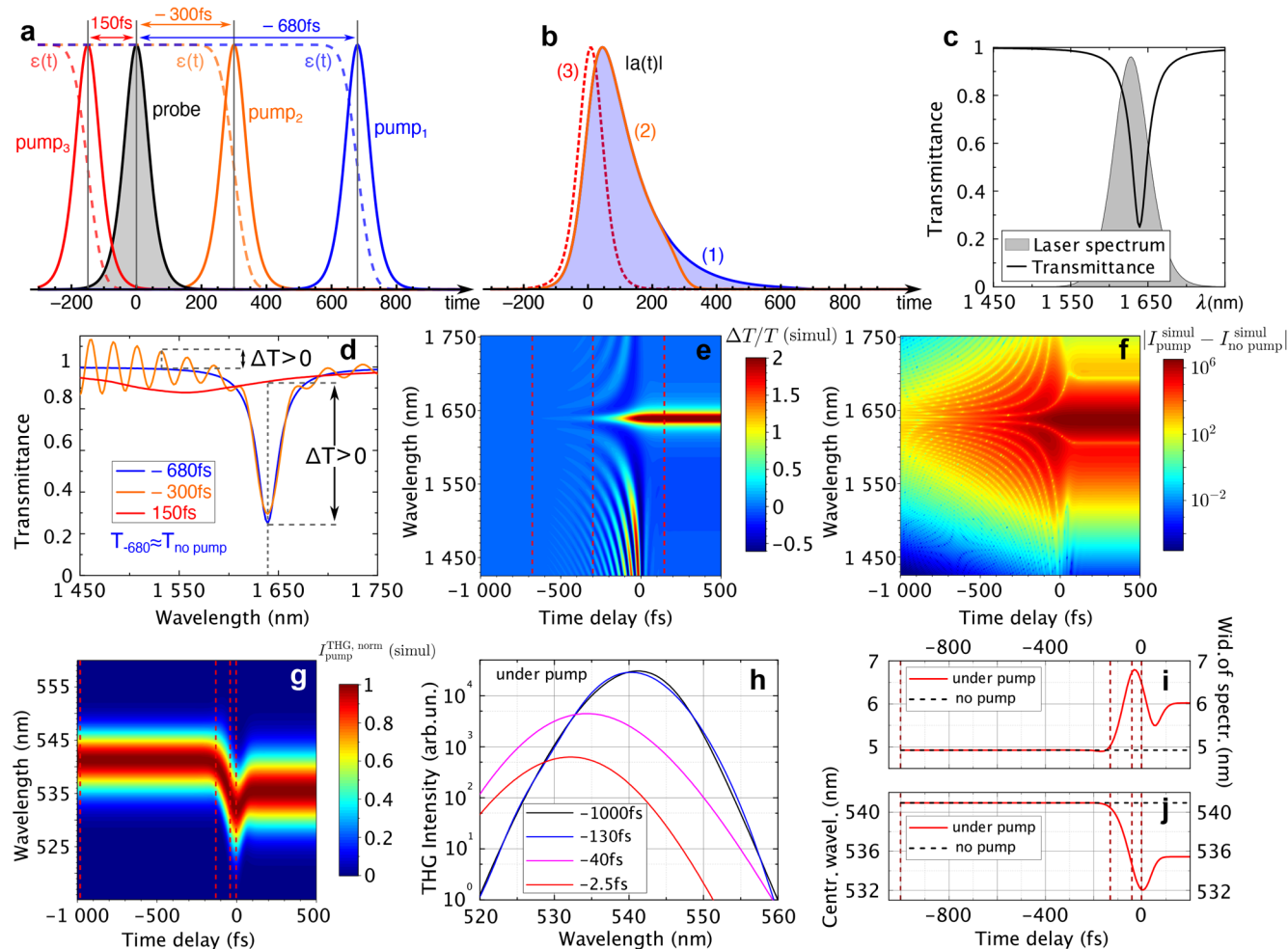


**Figure 4.** Coupled-mode theory results. (a) Temporal dynamics of pump–probe interaction for three main cases: pump<sub>1</sub> with pump–probe time delay  $\tau \ll \sigma_{\text{probe}}$  (blue curves in (a) and (b)), so in (d) the unperturbed resonance is observed (blue curve); pump<sub>2</sub> with negative  $\tau \approx 0$ , the resonance mode is present in the resonator, while the material properties are changed (orange curves in (a) and (b)); so the mode is transformed by the time-variant parameter and the fringes that indicate the frequency conversion occur in the transmittance spectrum (orange curve in (d)); pump<sub>3</sub> with  $\tau > 0$ , the probe arrives shortly after the pump makes changes in the material and both the blue-shift and reduced Q-factor of the resonance are observed in transmittance (red curve in (d)). Dashed curves display the pump-induced dielectric permittivity changes of the material  $\epsilon(t)$ . (b) Corresponding temporal dynamics of the resonance mode for the three cases. (c) The transmittance spectrum of the metasurface with the resonance at 1640 nm in the absence of optical pumping (black curve) and the spectrum of the probe pulse (gray region). (d) Transmittance spectra of the metasurface for tree main cases under pump. (e) Transient transmittance of the metasurface as a function of wavelength and pump–probe time delay. Red dashed lines denote the time delays used in (a), (b), and (d). (f) The difference between probe spectrum under pump illumination and without pump illumination as a function of wavelength and pump–probe time delay, logarithmic scale. (g) The normalized third-harmonic signal generated by the probe pulse under pump illumination. Red dashed lines in (g), (i), and (j) denote the time delays for the THG intensity spectra cross sections in (h). (h) THG spectra under pump illumination for some pump–probe delays; here  $I_{\text{pump}}^{\text{THG}}(-1000 \text{ fs}) = I_{\text{pump}}^{\text{THG}}(-1000 \text{ fs})$ . The fitting result of THG intensity by the  $\text{sech}^2$  function, eq 1, with spectral width  $\sigma$  (i) and central wavelength  $\lambda_0$  (j) under pump (red curves) and without pump illumination (dashed black curves).

corresponds to the frequency conversion of  $3.05\omega$  in comparison with unperturbed nonlinear signal that is expected at  $3\omega$ . The essence of the THG blue-shift effect is associated with the metasurface resonance blue-shift at the fundamental wavelength under pump illumination and subsequent redistribution of the frequency components of the third-harmonic spectrum. As shown in Figure 1b, the higher is the pump fluence, the larger is the blue-shift of the resonance. The nonlinear modulation of the a-Ge metasurface was measured at a pump fluence of  $3 \text{ mJ/cm}^2$  when the resonance shift is estimated to be about 100 nm. The main feature related to the shift of the resonance at the fundamental frequency occurs at a time scale of  $\sim -100 \text{ fs}$  since the region  $\tau$  between  $-200$  and  $0$

fs is characterized by the most pronounced and spectrally broad fringes (Figure 2a,b). Similar temporal dynamics one can observe in the nonlinear response as well. Finally, when the resonance shifts far enough from the fundamental spectrum center, near  $\tau = 0$ , the nonlinear response becomes highly impeded by the formed plasma; the signal for  $\tau > 0$  can no longer be detected under the same experimental conditions (hatched white rectangle area in Figure 3a).

**Theory.** We construct a time-dependent coupled-mode theory (CMT)<sup>58</sup> to confirm the description of our experiment and to get a better understanding of the metasurface's dynamics. This theory allows simulating the ultrafast all-optical modulation of the metasurface's resonant mode as a function

of both time delay between the pump–probe pulses and probe wavelength. The probe is the short  $\text{sech}^2$  pulse (Figure 4a,c, gray region) and the pump influence is imitated by time-dependent mode parameters: central frequency  $\omega_0(t)$  and damping factor  $\gamma(t)$ , which arise as a result of a change in the dielectric permittivity  $\epsilon(t)$  under the induced free-carriers (Figure 4a, dashed curves). There are three main cases for pump–probe time delays shown in Figure 4a,b,d. In the first case (pump<sub>1</sub>), with the pump–probe time delay  $\tau$  being much less than the duration of the probe pulse  $\sigma_{\text{probe}}$ , the pump pulse arrives at the metasurface after the probe has almost completely radiated out of the resonator (blue curve in Figure 4a,b) and the resonance is close to the unperturbed one (Figure 4d, blue curve). In the second case (pump<sub>2</sub>), with negative  $\tau$  near zero, due to the finite lifetime of the resonance, the mode excited while the material properties are changed (orange curves in Figure 4a,b). The mode is transformed by the time-variant metasurface, and the fringes that indicate the frequency conversion appear in the transmittance spectrum in Figure 4d (orange curve). In the third case (pump<sub>3</sub>), with  $\tau > 0$ , the probe arrives shortly after the pump made changes in the material; thus, the probe interacts with the material whose dielectric permittivity has changed, and both the blue-shift and the reduced Q-factor of the resonance are observed in the transmittance spectrum in Figure 4d (red curve). The given delay times for the main cases are marked by red dashed lines in Figure 4e.

The transmittance of the unperturbed mode is shown in Figure 4c and is quite similar to the transmittance of the experimental a-Ge metasurface (Figure 1b, black curve). The probe spectrum width  $\sigma = 50$  nm is also taken close to the experimental value of  $\sigma = 55$  nm (for more calculation details, see Methods). Figure 4e represents the calculated transient transmittance of the metasurface, which is in excellent agreement with the experiment. The region with high modulation values (dark red area at short wavelengths) occurs due to the division by small values of the unperturbed spectrum, and may not describe well the experimental probe spectrum as far as the spectral tails are concerned. This area can be clearly seen without division in Figure 4f, where the absolute difference between probe spectrum under pump illumination and without pump illumination is shown on a logarithmic scale. The corresponding normalized third-harmonic signal is given in Figure 4g. The signal reveals the blue-shift on a femtosecond scale as obtained in the experiment. The red dashed lines denote the time delays for the intensity spectra cross sections in Figure 4h. These cross sections of THG spectra under pump illumination display the blue-shifting and broadening of the spectra which increase at  $\tau \approx 0$ . The THG probe spectrum at  $\tau = -1000$  fs under pump (black curve) completely matches with the THG probe spectrum without pump in this region. The shift of the THG spectrum at positive time delays relative to the unperturbed spectrum without pump is related to the changed resonance properties of the media (red curve in Figure 4d), but is not associated with the time-variant nature of the system (see Supporting Information for the details).<sup>59</sup> The temporal dynamics for width of spectrum  $\sigma$  and central wavelength  $\lambda_0$  was obtained from fitting by  $\text{sech}^2$  function with eq 1 as a function of time delay between the pump–probe pulses (Figure 4i,j). The blue-shift reaches a maximum value of about 10 nm and the broadening is about 40%, which is in excellent agreement with the experimental values.

## DISCUSSION

A part of the probe pulse that couples to the metasurface stays with it for a time comparable to the lifetime of the mode. The powerful pump pulse arrives shortly after the mode is populated and generates free carriers, altering the refractive index of the semiconductor and shifting the resonance by up to 100 nm at a pump fluence of 3 mJ/cm<sup>2</sup>. This shift, along with the dynamic widening of the resonance, enables broadband frequency conversion at up to 200 nm away from the carrier wavelength at negative time delays in pump–probe traces.

Due to the high values of the intrinsic third-order nonlinear susceptibility  $\chi^{(3)}$  of a-Ge, one can observe the third-harmonic signal generated by the probe pulse in the a-Ge material. The THG is described by the nonlinear polarization  $\mathbf{P}_{\text{NL}}^{(3)}(3\omega) = \epsilon_0 \chi^{(3)}(3\omega) \mathbf{E}(\omega) \mathbf{E}(\omega) \mathbf{E}(\omega)$ , and owing to the electric field enhancement in the metasurface, the THG signal is observed at a lower power compared to the bulk a-Ge. The femtosecond-scale changes in the fundamental beam spectrum lead to the femtosecond changes in the third-harmonic signal generated by the probe pulse and revealed in the blue-shift and broadening of the third-harmonic spectrum. While this observation is deemed possible in high-Q metasurfaces, our modeling shows that the femtosecond dynamics of THG at negative time delays  $\tau < 0$  displayed in Figure 3 is significantly smaller for lower Q-factors, see Supporting Information, Figure S1. Since in the CMT calculations we used pulses of the same duration as in the experiment, we expected to see the maximum value of the THG blue-shift at delays  $\sim -100$  fs time scale. In addition, the four-wave mixing (FWM) process:  $2\omega_{\text{pump}} - \omega_{\text{probe}}$  for the fundamental probe wavelength  $\lambda_{\text{probe}} = 1610$  nm and the pump wavelength  $\lambda_{\text{pump}} = 800$  nm yields a resulting wavelength  $\lambda_{\text{FWM}} \approx 530$  nm that is close to the maximum achieved shifted THG. To exclude the influence of the FWM, we measured the THG signal for  $\lambda_{\text{probe}} = 1670$  nm for the case when both the fundamental probe wavelength located close to the metasurface resonance, and it is possible to separate the THG and FWM processes ( $\lambda_{\text{THG}} \approx 560$  nm,  $\lambda_{\text{FWM}} \approx 525$  nm). As a result, the FWM process does not manifest itself and does not affect the measured visible response (see Supporting Information, Figure S2), and we can conclude that the measured nonlinear signal is attributed to the THG. Moreover, we use the pump–probe scheme with different pump and probe wavelengths, and so we expect that coherent artifacts occurring in such experiments at near-zero time delays due to the interference of pump and probe<sup>60</sup> beams cannot be observed in our experiment. Our results pinpoint the significance of high-Q resonances in the processes of frequency conversion in time-variant metasurfaces and serve as an important step to the full understanding of this phenomenon.

To conclude, we have designed, fabricated, and studied an a-Ge-based metasurface that exhibits photoinduced frequency conversion via a high-Q resonance with rapidly varying parameters. Pump–probe experiments show pronounced spectral features in the probe beam and its third optical harmonic at negative pump–probe delay times. In the first observation of switching and frequency tuning of a harmonic signal in a semiconductor metasurface, we demonstrated a 10 nm blue-shift and 40% broadening of its spectrum on the subpicosecond time scale at negative pump–probe delays and almost complete suppression of the THG at positive delays. The observed blue-shift and broadening are caused by the pump-induced dynamics of the high-Q factor metasurface



resonance, as confirmed by coupled-mode theory calculations. Nonlinear time-variant metasurfaces represent a promising novel class of artificial semiconductor nanostructures that can serve as the base for new-generation pulse shapers, optical switches, and light sources.

## METHODS

**Sample Fabrication.** Samples of germanium metasurfaces were fabricated by thermal deposition of a thin (200 nm) a-Ge film on a CaF<sub>2</sub> substrate, subject to electron beam lithography with 100 nm-thick HSQ resist exposed at a dose of 800  $\mu\text{C}/\text{cm}^2$ , development in TMAH (120 s, 3% solution), and reactive ion etching in SF<sub>6</sub> plasma. The total dimensions of the nanostructured areas were 500  $\times$  500  $\mu\text{m}^2$ .

**Sample Characterization.** Near-infrared spectroscopy of the samples was performed using a home-built setup. The beam from an incandescent light source was focused to a spot size of about 300  $\mu\text{m}$  with a numerical aperture of NA = 0.05. The transmitted beam was analyzed by an IR InGaAs CCD-based spectrometer. Normalization was done by the spectrum of the source with the sample removed from the optical path. The setup allowed measuring transmittance for different angles of incidence and linear polarization states of the incident light. The resonances with high Q-factors were observed for the polarization orientation of the incident light perpendicular to the long sides of the a-Ge cuboids.

**Pump–Probe Spectroscopy.** A Ti:sapphire regenerative amplifier (Coherent Libra) serving as a pump and an optical parametric amplifier (OPA) serving as a probe were used to investigate frequency conversion in the semiconductor metasurface. The pump was a 60 fs laser pulses train (as measured using an autocorrelator) of 800 nm wavelength with 1 kHz repetition rate. Its average power was varied using a variable optical density filter from 0.5 to 6 mW, while retaining a spot size of about 500  $\mu\text{m}$  in diameter in the sample plane. We chose the pump wavelength  $\lambda_{\text{pump}} = 800$  nm because its photon energy  $E_{\text{pump}} = 1.55$  eV is larger than a-Ge band gap  $E_g$ , so that the linear absorption is dominant over the higher-order absorption processes in a-Ge. The probe was a 50 fs pulses train with 1 kHz repetition rate and wavelength tunable in the range from 1610 to 1670 nm, with an average beam power of about 40 mW. Both beams were *p*-polarized at the metasurface plane. The duration of the probe was measured by a cross-correlation scheme with the use of a pump as one of the pulses and using a BBO nonlinear crystal that produced a sum-frequency beam. The transmitted probe pulse spectra (or third-harmonic generated by the probe) were measured as a function of both time delay between the pump and probe pulses and the probe fundamental wavelength (or THG wavelength) under and without pump presence by a near-IR spectrometer (or visible spectrometer). In order to increase the signal-to-noise ratio of the measured third-harmonic spectra, a probe of higher intensity in comparison with linear measurements was used. The high intensity of the probe leads to the noticeable change in the quality factor of the resonance due to the increased nonradiative losses under free-carriers generated in Ge. In our case, the used intensity level resulted in the decrease of the Q-factor almost 2 times from the initial and the Q-factor of the resonance became equal to 30. In addition to this, the central wavelength of the probe was shifted from  $\lambda = 1640$  (used in linear measurements) to 1610 nm to increase the signal-to-noise ratio of the “red”-part of the blue-shifted generated THG spectra. The measurements were carried out

with a frequency from 0.1 to 50 Hz depending on the averaging time of the spectrometer. A normalized 3D map of THG intensity was obtained by normalizing the spectrum at each pump–probe time delay to its maximum. The area with noisy signal that prevents meaningful normalization have artificially low values and is shown by the hatched white rectangle in Figure 3a. The normalized intensity of THG was used for a clearer observation of the signal blue-shift due to the decreasing of the signal value with increasing time delay of pump–probe and due to the instability of the probe laser. The main fingerprints of the time-variance in the system (the central wavelength and the spectrum width) are not connected to the intensity instability of the probe beam. According to the predictions by the CMT, we expected to see the maximum value of the THG blue-shift at delays around  $-100$  fs time scale, which is indeed seen in the experimental results.

**FDTD Simulations.** The transmittance spectra were calculated using a commercial Lumerical FDTD Solutions software for an a-Ge metasurface with the following parameters: the dimensions of the cuboid short side  $x = 360$  nm, long side  $y = 753$  nm, the period along the  $Ox$  axis  $P_x = 1035$  nm, along the  $Oy$  axis  $P_y = 1060$  nm and the a-Ge layer thickness of 140 nm. The characteristic geometric parameters was achieved from the SEM image of the sample. There was a residual silica cap due to the fabrication process on top of the a-Ge cuboid. We used a nondispersive dielectric material with  $n = 1.6$  and  $h_{\text{SiO}_2} = 100$  nm for this cap and  $n = 1.45$  for the CaF<sub>2</sub> substrate. For the a-Ge material, we used the available tabulated experimental data.<sup>61</sup> Periodic boundary conditions were used to simulate periodic structure of metasurface and perfectly matched layer (PML) conditions were used in the  $z$  direction. The plane wave excitation was from the top at a normal angle with the polarization perpendicular to the long sides of the cuboids, as shown by a white arrow in the SEM image of the sample in Figure 1c.

**CMT Calculations.** The experimental data can be understood in terms of a time-dependent coupled-mode theory.<sup>58</sup> We considered a single resonant mode being excited by a short pulse, for which CMT gives the following equation:

$$\dot{a}(t) + [i\omega(t) + \gamma_{\text{nr}}(t) + \gamma_{\text{r}}]a(t) = \sqrt{\gamma_{\text{r}}}s(t) \quad (2)$$

Here,  $a(t)$  is the complex amplitude of the exited mode,  $\omega$  is the resonant frequency of the mode,  $\gamma_{\text{r}}$  and  $\gamma_{\text{nr}}$  are the radiative and nonradiative contributions to the decay rate, and  $s(t)$  is the exciting pulse. We added a time dependence to the properties of our mode ( $\gamma_{\text{nr}}$  and  $\omega$ ) to model the effects of the pump. We use a  $\text{sech}^2$  excitation pulse:  $s(t) = \text{sech}^2((t)/\sigma_{\text{probe}}) \exp[-i\omega_{\text{probe}}t]$ , where  $\sigma_{\text{probe}}$  controlled the width of the pulse and  $\omega_{\text{probe}}$  corresponded to the central frequency.

We determined the time dependence of the resonant mode by the following consideration. Since we used a short pump pulse with a Gaussian-type profile to excite free carriers in the metasurface, the change in the dielectric permittivity of germanium could be approximated by the error function:  $\epsilon(t) = \epsilon_{\infty} + \Delta\epsilon/2[\text{erf}[(t + \tau)/\sigma_{\text{pump}}] + 1]$ , where  $\epsilon_{\infty}$  is the permittivity without the pump,  $\Delta\epsilon$  is the total change induced in the material,  $\tau$  is the pump arrival time, and  $\sigma_{\text{pump}}$  is the duration of the pump pulse. Here the model does not take into account the relaxation processes of free carriers, since the typical relaxation time is longer than the studied one. Assuming that the mode resonant frequency is linearly dependent on the permittivity, we can write the same equation

for  $\omega$  by substituting  $\epsilon_{-\infty}$  for the unperturbed resonant frequency  $\omega_{-\infty}$  and  $\Delta\epsilon$  for the change in resonant frequency  $\Delta\omega$ :

$$\omega(t) = \omega_{-\infty} + \frac{\Delta\omega}{2} \left[ \operatorname{erf} \left( \frac{t + \tau}{\sigma_{\text{pump}}} \right) + 1 \right] \quad (3)$$

In addition to changing the resonant frequency, the free carriers also add absorption, which leads to a change in  $\gamma_{\text{nr}}$ . Since permittivity and absorption generally have the same dependence on the free carrier concentration, here we assumed that  $\gamma_{\text{nr}}(t)$  behaved the same way that  $\omega(t)$  did:  $\gamma_{\text{nr}}(t) - \gamma_{\text{nr}-\infty} = \xi(\omega(t) - \omega_{-\infty})$ , where  $\gamma_{\text{nr}-\infty}$  is the unperturbed nonradiative decay rate and  $\xi$  is a numeric coefficient that is determined by the material used for the resonator. Since the correct value of  $\xi$  is unknown for a-Ge, we performed these simulations for various values from  $\xi = 0.5$  to 2. We found that  $\xi = 1$  yielded results closest to the experimental measurements, so we used this value for all the data presented here. Since the relative change of the refractive index of a-Ge is small, we assumed that the mode profile remains largely unchanged, and  $\gamma_r$  did not change significantly in the process, so we take it to be constant.

Equation 2 was numerically solved using the explicit Runge–Kutta method as implemented in the NDSolve function from Wolfram Mathematica computation engine. The parameters we used were close to the experimental ones:  $\omega_{-\infty} = 1150$  THz ( $\lambda_{-\infty} = 1640$  nm),  $\Delta\omega = 63$  THz ( $\Delta\lambda = 100$  nm),  $\sigma_{\text{probe}} = \sigma_{\text{pump}} = 50$  fs,  $\omega_{\text{probe}} = 1158$  THz ( $\lambda = 1628$  nm, for linear calculations) and 1171 THz ( $\lambda = 1610$  nm, for nonlinear calculations),  $\gamma_{\text{nr}-\infty} = 4.5$  THz,  $\gamma_r = 4.5$  THz (equivalent to  $Q = 65$  for linear calculations) and 8 THz (equivalent to  $Q = 36.6$  for nonlinear calculations). The two different decay rates and central wavelengths were used due to the different probe intensities and wavelengths used in the linear and nonlinear experiments. Due to difficulty in measuring the third-harmonic spectra, a probe of higher intensity at  $\lambda = 1610$  nm was used in nonlinear experiments, generating free carriers in germanium increasing the non-radiative losses. A much weaker probe at  $\lambda = 1628$  nm is used in linear experiments, leading to no noticeable changes in the quality factor of the resonance. To model the pump–probe experiment, the pump arrival time  $\tau$  from eq 3 is varied between  $\tau = -1000$  and 500 fs.

The light radiated by the mode can be obtained using the following equation:  $s_r(t) = s(t) - \sqrt{\gamma_r} a(t)$ . We then performed a Fourier transform:  $I^{\text{simul}}(\omega) = \text{abs}[F[s_r(t)]]^2$ , where  $I^{\text{simul}}(\omega)$  is the simulated transmission spectrum and  $F$  denotes the Fourier transform. The resulting transient transmission spectra as a function of the delay between the probe and the pump are shown in Figure 4e. By performing the same calculation without any temporal changes to the resonant mode, we get the spectrum for the case when there is no pump present (the transmission in this case is indicated with a black curve on Figure 4c), then we can plot the same value as presented in experimental results  $|I_{\text{pump}}^{\text{simul}} - I_{\text{no\_pump}}^{\text{simul}}|$  (Figure 4f).

To simulate the third-harmonic generation, the real part of the complex amplitude of the resonant mode was raised to the third power:  $I^{\text{THG}}(\omega) = \text{abs}[F(\text{Re}[a(t)]^3)]^2$ . Although this approach ignores several important effects that influence third-harmonic generation in the system, it gives a good estimate of frequency conversion in the third-harmonic generation spectrum. The normalized calculated nonlinear spectra are

demonstrated in Figure 4g. The spectra for several pump–probe delays are displayed in Figure 4h on the logarithmic scale, where a blue-shift of the spectrum is clearly seen as the delay approaches zero. By fitting these spectra with a  $\text{sech}^2$  function, we estimate the width and central wavelength of the spectra, these results are shown in Figure 4i,j.

These simulation results provide qualitative agreement with experimental data in both linear and the third-harmonic spectra. We see the same periodic modulations in the linear spectra that stretch far from the original probe spectrum (Figure 4f). In third-harmonic simulations, we observe a shift in central frequency of 10 nm and a widening of the spectrum by approximately 40%, which is very close to the experimental results.

## ■ ASSOCIATED CONTENT

### Supporting Information

The Supporting Information is available free of charge at <https://pubs.acs.org/doi/10.1021/acsphotonics.1c01222>.

CMT calculations for different resonance Q-factors and different pump fluence, nonlinear response for different fundamental probe wavelengths, and nonlinear response for different metasurfaces (PDF)

## ■ AUTHOR INFORMATION

### Corresponding Author

Varvara V. Zubyyuk – Faculty of Physics, Lomonosov Moscow State University, Moscow 119991, Russia; [orcid.org/0000-0003-2337-4905](https://orcid.org/0000-0003-2337-4905); Email: [zubyyuk@nanolab.phys.msu.ru](mailto:zubyyuk@nanolab.phys.msu.ru)

### Authors

Pavel A. Shafirin – Faculty of Physics, Lomonosov Moscow State University, Moscow 119991, Russia

Maxim R. Shcherbakov – Faculty of Physics, Lomonosov Moscow State University, Moscow 119991, Russia; School of Applied and Engineering Physics, Ithaca, New York 14853, United States; [orcid.org/0000-0001-7198-5482](https://orcid.org/0000-0001-7198-5482)

Gennady Shvets – School of Applied and Engineering Physics, Ithaca, New York 14853, United States

Andrey A. Fedyanin – Faculty of Physics, Lomonosov Moscow State University, Moscow 119991, Russia; [orcid.org/0000-0003-4708-6895](https://orcid.org/0000-0003-4708-6895)

Complete contact information is available at: <https://pubs.acs.org/10.1021/acsphotonics.1c01222>

### Notes

The authors declare no competing financial interest.

## ■ ACKNOWLEDGMENTS

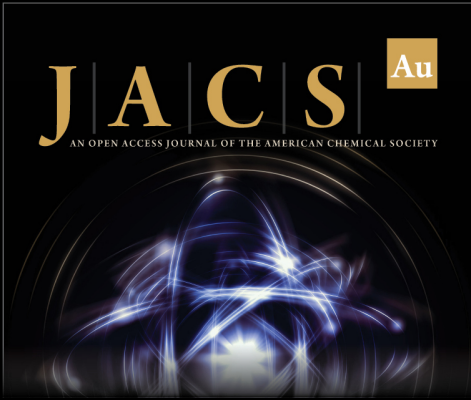
The work was supported by Russian Science Foundation (18-12-00475, optical measurements and coupled-mode theory) and Ministry of Science and Higher Education of Russian Federation (14.W03.31.0008, linear spectroscopy and FDTD simulation). The research was partly supported by MSU Quantum Technology Centre. The fabrication effort was carried out at the Cornell NanoScale Facility, a member of the National Nanotechnology Coordinated Infrastructure (NNCI), which is supported by the National Science Foundation (Grant NNCI-2025233).




## REFERENCES


- (1) Kuznetsov, A. I.; Miroshnichenko, A. E.; Brongersma, M. L.; Kivshar, Y. S.; Luk'yanchuk, B. Optically resonant dielectric nanostructures. *Science* **2016**, *354*, aag2472.
- (2) Yu, N.; Capasso, F. Flat optics with designer metasurfaces. *Nat. Mater.* **2014**, *13*, 139–150.
- (3) Khorasaninejad, M.; Capasso, F. Metalenses: Versatile multifunctional photonic components. *Science* **2017**, *358*, eaam8100.
- (4) Ni, X.; Kildishev, A. V.; Shalaev, V. M. Metasurface holograms for visible light. *Nat. Commun.* **2013**, *4*, 2807.
- (5) Zheng, G.; Mühlenbernd, H.; Kenney, M.; Li, G.; Zentgraf, T.; Zhang, S. Metasurface holograms reaching 80% efficiency. *Nat. Nanotechnol.* **2015**, *10*, 308–312.
- (6) Wang, L.; Kruk, S.; Koshelev, K.; Kravchenko, I.; Luther-Davies, B.; Kivshar, Y. Nonlinear wavefront control with all-dielectric metasurfaces. *Nano Lett.* **2018**, *18*, 3978–3984.
- (7) Zhou, Z.; Li, J.; Su, R.; Yao, B.; Fang, H.; Li, K.; Zhou, L.; Liu, J.; Stellinga, D.; Reardon, C. P.; et al. Efficient silicon metasurfaces for visible light. *ACS Photonics* **2017**, *4*, 544–551.
- (8) Shcherbakov, M. R.; Neshev, D. N.; Hopkins, B.; Shorokhov, A. S.; Staude, I.; Melik-Gaykazyan, E. V.; Decker, M.; Ezhov, A. A.; Miroshnichenko, A. E.; Brener, I.; et al. Enhanced third-harmonic generation in silicon nanoparticles driven by magnetic response. *Nano Lett.* **2014**, *14*, 6488–6492.
- (9) Makarov, S.; Kudryashov, S.; Mukhin, I.; Mozharov, A.; Milichko, V.; Krasnok, A.; Belov, P. Tuning of magnetic optical response in a dielectric nanoparticle by ultrafast photoexcitation of dense electron-hole plasma. *Nano Lett.* **2015**, *15*, 6187–6192.
- (10) Grinblat, G.; Li, Y.; Nielsen, M. P.; Oulton, R. F.; Maier, S. A. Enhanced third harmonic generation in single germanium nanodisks excited at the anapole mode. *Nano Lett.* **2016**, *16*, 4635–4640.
- (11) Shibamura, T.; Grinblat, G.; Albella, P.; Maier, S. A. Efficient third harmonic generation from metal-dielectric hybrid nanoantennas. *Nano Lett.* **2017**, *17*, 2647–2651.
- (12) Semmlinger, M.; Tseng, M. L.; Yang, J.; Zhang, M.; Zhang, C.; Tsai, W.-Y.; Tsai, D. P.; Nordlander, P.; Halas, N. J. Vacuum ultraviolet light-generating metasurface. *Nano Lett.* **2018**, *18*, 5738–5743.
- (13) Liu, S.; Vabishchevich, P. P.; Vaskin, A.; Reno, J. L.; Keeler, G. A.; Sinclair, M. B.; Staude, I.; Brener, I. An all-dielectric metasurface as a broadband optical frequency mixer. *Nat. Commun.* **2018**, *9*, 2507.
- (14) Liu, H.; Guo, C.; Vampa, G.; Zhang, J. L.; Sarmiento, T.; Xiao, M.; Bucksbaum, P. H.; Vučković, J.; Fan, S.; Reis, D. A. Enhanced high-harmonic generation from an all-dielectric metasurface. *Nat. Phys.* **2018**, *14*, 1006–1010.
- (15) Sain, B.; Meier, C.; Zentgraf, T. Nonlinear optics in all-dielectric nanoantennas and metasurfaces: a review. *Adv. Photonics* **2019**, *1*, 024002.
- (16) Holsteen, A. L.; Raza, S.; Fan, P.; Kik, P. G.; Brongersma, M. L. Purcell effect for active tuning of light scattering from semiconductor optical antennas. *Science* **2017**, *358*, 1407–1410.
- (17) Park, J.; Kang, J.-H.; Kim, S. J.; Liu, X.; Brongersma, M. L. Dynamic reflection phase and polarization control in metasurfaces. *Nano Lett.* **2017**, *17*, 407–413.
- (18) Shirmanesh, G. K.; Sokhoyan, R.; Wu, P. C.; Atwater, H. A. Electro-optically tunable multifunctional metasurfaces. *ACS Nano* **2020**, *14*, 6912–6920.
- (19) Rahmani, M.; Xu, L.; Miroshnichenko, A. E.; Komar, A.; Camacho-Morales, R.; Chen, H.; Zárate, Y.; Kruk, S.; Zhang, G.; Neshev, D. N.; et al. Reversible thermal tuning of all-dielectric metasurfaces. *Adv. Funct. Mater.* **2017**, *27*, 1700580.
- (20) Yang, Y.; Wang, W.; Boulesbaa, A.; Kravchenko, I. I.; Briggs, D. P.; Puretzky, A.; Geoghegan, D.; Valentine, J. Nonlinear Fano-resonant dielectric metasurfaces. *Nano Lett.* **2015**, *15*, 7388–7393.
- (21) Shcherbakov, M. R.; Vabishchevich, P. P.; Shorokhov, A. S.; Chong, K. E.; Choi, D.-Y.; Staude, I.; Miroshnichenko, A. E.; Neshev, D. N.; Fedyanin, A. A.; Kivshar, Y. S. Ultrafast all-optical switching with magnetic resonances in nonlinear dielectric nanostructures. *Nano Lett.* **2015**, *15*, 6985–6990.
- (22) Shcherbakov, M. R.; Liu, S.; Zubyuk, V. V.; Vaskin, A.; Vabishchevich, P. P.; Keeler, G.; Pertsch, T.; Dolgova, T. V.; Staude, I.; Brener, I.; Fedyanin, A. A. Ultrafast all-optical tuning of direct-gap semiconductor metasurfaces. *Nat. Commun.* **2017**, *8*, 17.
- (23) Zubritskaya, I.; Maccaferri, N.; Inchausti Ezeiza, X.; Vavassori, P.; Dmitriev, A. Magnetic control of the chiroptical plasmonic surfaces. *Nano Lett.* **2018**, *18*, 302–307.
- (24) Barsukova, M. G.; Musorin, A. I.; Shorokhov, A. S.; Fedyanin, A. A. Enhanced magneto-optical effects in hybrid Ni-Si metasurfaces. *APL Photonics* **2019**, *4*, 016102.
- (25) Musorin, A. I.; Chetvertukhin, A. V.; Dolgova, T. V.; Uchida, H.; Inoue, M.; Luk'yanchuk, B. S.; Fedyanin, A. A. Tunable multimodal magnetoplasmonic metasurfaces. *Appl. Phys. Lett.* **2019**, *115*, 151102.
- (26) Gholipour, B.; Zhang, J.; MacDonald, K. F.; Hewak, D. W.; Zheludev, N. I. An all-optical, non-volatile, bidirectional, phase-change meta-switch. *Adv. Mater. Lett.* **2013**, *25*, 3050–3054.
- (27) Karvounis, A.; Gholipour, B.; MacDonald, K. F.; Zheludev, N. I. All-dielectric phase-change reconfigurable metasurface. *Appl. Phys. Lett.* **2016**, *109*, 051103.
- (28) Di Martino, G.; Tappertzhofen, S.; Hofmann, S.; Baumberg, J. Nanoscale Plasmon-Enhanced Spectroscopy in Memristive Switches. *Small* **2016**, *12*, 1334–1341.
- (29) Sautter, J.; Staude, I.; Decker, M.; Rusak, E.; Neshev, D. N.; Brener, I.; Kivshar, Y. S. Active tuning of all-dielectric metasurfaces. *ACS Nano* **2015**, *9*, 4308–4315.
- (30) Komar, A.; Fang, Z.; Bohn, J.; Sautter, J.; Decker, M.; Miroshnichenko, A.; Pertsch, T.; Brener, I.; Kivshar, Y. S.; Staude, I.; et al. Electrically tunable all-dielectric optical metasurfaces based on liquid crystals. *Appl. Phys. Lett.* **2017**, *110*, 071109.
- (31) Kruk, S.; Kivshar, Y. Functional meta-optics and nanophotonics governed by Mie resonances. *ACS Photonics* **2017**, *4*, 2638–2649.
- (32) Staude, I.; Miroshnichenko, A. E.; Decker, M.; Fofang, N. T.; Liu, S.; Gonzales, E.; Dominguez, J.; Luk, T. S.; Neshev, D. N.; Brener, I.; et al. Tailoring directional scattering through magnetic and electric resonances in subwavelength silicon nanodisks. *ACS Nano* **2013**, *7*, 7824–7832.
- (33) Neuner, B., III; Wu, C.; Eyck, G. T.; Sinclair, M.; Brener, I.; Shvets, G. Efficient infrared thermal emitters based on low-albedo polaritonic meta-surfaces. *Appl. Phys. Lett.* **2013**, *102*, 211111.
- (34) Sui, C.; Li, X.; Lang, T.; Jing, X.; Liu, J.; Hong, Z. High Q-factor resonance in a symmetric array of all-dielectric bars. *Appl. Sci.* **2018**, *8*, 161.
- (35) Shalaev, M. I.; Sun, J.; Tsukernik, A.; Pandey, A.; Nikolskiy, K.; Litchinitser, N. M. High-efficiency all-dielectric metasurfaces for ultracompact beam manipulation in transmission mode. *Nano Lett.* **2015**, *15*, 6261–6266.
- (36) Liu, Y.; Zhou, W.; Sun, Y. Optical refractive index sensing based on high-Q bound states in the continuum in free-space coupled photonic crystal slabs. *Sensors* **2017**, *17*, 1861.
- (37) Reshef, O.; Saad-Bin-Alam, M.; Huttunen, M. J.; Carlow, G.; Sullivan, B. T.; Ménard, J.-M.; Dolgaleva, K.; Boyd, R. W. Multiresonant High-Q Plasmonic Metasurfaces. *Nano Lett.* **2019**, *19*, 6429–6434.
- (38) Zubyuk, V. V.; Vabishchevich, P. P.; Shcherbakov, M. R.; Shorokhov, A. S.; Fedotova, A. N.; Liu, S.; Keeler, G.; Dolgova, T. V.; Staude, I.; Brener, I.; et al. Low-power absorption saturation in semiconductor metasurfaces. *ACS Photonics* **2019**, *6*, 2797–2806.
- (39) Shcherbakov, M. R.; Werner, K.; Fan, Z.; Talisa, N.; Chowdhury, E.; Shvets, G. Photon acceleration and tunable broadband harmonics generation in nonlinear time-dependent metasurfaces. *Nat. Commun.* **2019**, *10*, 1345.
- (40) Lee, K.; Son, J.; Park, J.; Kang, B.; Jeon, W.; Rotermund, F.; Min, B. Linear frequency conversion via sudden merging of meta-atoms in time-variant metasurfaces. *Nat. Photonics* **2018**, *12*, 765–773.
- (41) Lee, K.; Park, J.; Son, J.; Kang, B. J.; Kim, W. T.; Lee, S. C.; Min, B.; Rotermund, F. Electrical control of terahertz frequency


- conversion from time-varying surfaces. *Opt. Express* **2019**, *27*, 12762–12773.
- (42) Karl, N.; Vabishchevich, P. P.; Shcherbakov, M. R.; Liu, S.; Sinclair, M. B.; Shvets, G.; Brener, I. Frequency Conversion in a Time-Variant Dielectric Metasurface. *Nano Lett.* **2020**, *20*, 7052–7058.
- (43) Guo, X.; Ding, Y.; Duan, Y.; Ni, X. Nonreciprocal metasurface with space-time phase modulation. *Light: Sci. Appl.* **2019**, *8*, 123.
- (44) Zang, J. W.; Correias-Serrano, D.; Do, J.; Liu, X.; Alvarez-Melcon, A.; Gomez-Diaz, J. S. Nonreciprocal wavefront engineering with time-modulated gradient metasurfaces. *Phys. Rev. Appl.* **2019**, *11*, 054054.
- (45) Cardin, A. E.; Silva, S. R.; Vardeny, S. R.; Padilla, W. J.; Saxena, A.; Taylor, A. J.; Kort-Kamp, W. J.; Chen, H.-T.; Dalvit, D. A.; Azad, A. K. Surface-wave-assisted nonreciprocity in spatio-temporally modulated metasurfaces. *Nat. Commun.* **2020**, *11*, 1469.
- (46) Kuo, S. P. Frequency up-conversion of microwave pulse in a rapidly growing plasma. *Phys. Rev. Lett.* **1990**, *65*, 1000.
- (47) Dias, J. M.; Stenz, C.; Lopes, N.; Badiche, X.; Blasco, F.; Dos Santos, A.; Oliveira e Silva, L.; Mysyrowicz, A.; Antonetti, A.; Mendonca, J. T. Experimental evidence of photon acceleration of ultrashort laser pulses in relativistic ionization fronts. *Phys. Rev. Lett.* **1997**, *78*, 4773.
- (48) Hamm, P. Coherent effects in femtosecond infrared spectroscopy. *Chem. Phys.* **1995**, *200*, 415–429.
- (49) Yan, S.; Seidel, M. T.; Tan, H.-S. Perturbed free induction decay in ultrafast mid-IR pump-probe spectroscopy. *Chem. Phys. Lett.* **2011**, *517*, 36–40.
- (50) Fluegel, B.; Peyghambarian, N.; Olbright, G.; Lindberg, M.; Koch, S. W.; Joffe, M.; Hulin, D.; Migus, A.; Antonetti, A. Femtosecond studies of coherent transients in semiconductors. *Phys. Rev. Lett.* **1987**, *59*, 2588.
- (51) Joffe, M.; Hulin, D.; Migus, A.; Antonetti, A.; Benoit à la Guillaume, C.; Peyghambarian, N.; Lindberg, M.; Koch, S. W. Coherent effects in pump-probe spectroscopy of excitons. *Opt. Lett.* **1988**, *13*, 276–278.
- (52) Utikal, T.; Stockman, M. I.; Heberle, A. P.; Lippitz, M.; Giessen, H. All-optical control of the ultrafast dynamics of a hybrid plasmonic system. *Phys. Rev. Lett.* **2010**, *104*, 113903.
- (53) Shorokhov, A. S.; Okhlopkov, K. I.; Reinhold, J.; Helgert, C.; Shcherbakov, M. R.; Pertsch, T.; Fedyanin, A. A. Ultrafast control of third-order optical nonlinearities in fishnet metamaterials. *Sci. Rep.* **2016**, *6*, 28440.
- (54) Sartorello, G.; Olivier, N.; Zhang, J.; Yue, W.; Gosztola, D. J.; Wiederrecht, G. P.; Wurtz, G.; Zayats, A. V. Ultrafast optical modulation of second-and third-harmonic generation from cut-disk-based metasurfaces. *ACS Photonics* **2016**, *3*, 1517–1522.
- (55) Cheng, Y.; Hong, H.; Zhao, H.; Wu, C.; Pan, Y.; Liu, C.; Zuo, Y.; Zhang, Z.; Xie, J.; Wang, J.; et al. Ultrafast Optical Modulation of Harmonic Generation in Two-Dimensional Materials. *Nano Lett.* **2020**, *20*, 8053–8058.
- (56) Shcherbakov, M. R.; Shafirin, P.; Shvets, G. Overcoming the efficiency-bandwidth tradeoff for optical harmonics generation using nonlinear time-variant resonators. *Phys. Rev. A* **2019**, *100*, 063847.
- (57) Shcherbakov, M. R.; Lemasters, R.; Fan, Z.; Song, J.; Lian, T.; Harutyunyan, H.; Shvets, G. Time-variant metasurfaces enable tunable spectral bands of negative extinction. *Optica* **2019**, *6*, 1441–1442.
- (58) Haus, H. A. *Waves And Fields In Optoelectronics*; Prentice-Hall, Inc.: Englewood Cliffs, NJ, 1984.
- (59) Vabishchevich, P. P.; Liu, S.; Sinclair, M. B.; Keeler, G. A.; Peake, G. M.; Brener, I. Enhanced second-harmonic generation using broken symmetry III–V semiconductor fano metasurfaces. *ACS Photonics* **2018**, *5*, 1685–1690.
- (60) Vardeny, Z.; Tauc, J. Picosecond coherence coupling in the pump and probe technique. *Opt. Commun.* **1981**, *39*, 396–400.
- (61) Palik, E. D. *Handbook Of Optical Constants Of Solids*; Academic Press: San Diego, CA, 1998; Vol. 3.



**JACS** <sup>Au</sup>  
AN OPEN ACCESS JOURNAL OF THE AMERICAN CHEMICAL SOCIETY

 Editor-in-Chief  
**Prof. Christopher W. Jones**  
Georgia Institute of Technology, USA

**Open for Submissions** 

pubs.acs.org/jacsau  **ACS Publications**  
Most Trusted. Most Cited. Most Read.